FuseSR: Super Resolution for Real-time Rendering through Efficient Multi-resolution Fusion

Zhihua Zhong*
zhongzhihua@zju.edu.cn
State Key Lab of CAD&CG,
Zhejiang University
Zhejiang University City
College
China

Jingsen Zhu*
zhujingsen@zju.edu.cn
State Key Lab of CAD&CG,
Zhejiang University
China

Yuxin Dai
buttersdyx@gmail.com
Zhejiang A&F University
China

Chuankun Zheng
ckzheng0320@zju.edu.cn
State Key Lab of CAD&CG,
Zhejiang University
China

Yuchi Huo†
huo.yuchi.sc@gmail.com
Zhejiang Lab
State Key Lab of CAD&CG,
Zhejiang University
China

Guanlin Chen
chenguanlin@zucc.edu.cn
Zhejiang University City
College
China

Hujun Bao
bao@cad.zju.edu.cn
State Key Lab of CAD&CG,
Zhejiang University
China

Rui Wang†
rwang@cad.zju.edu.cn
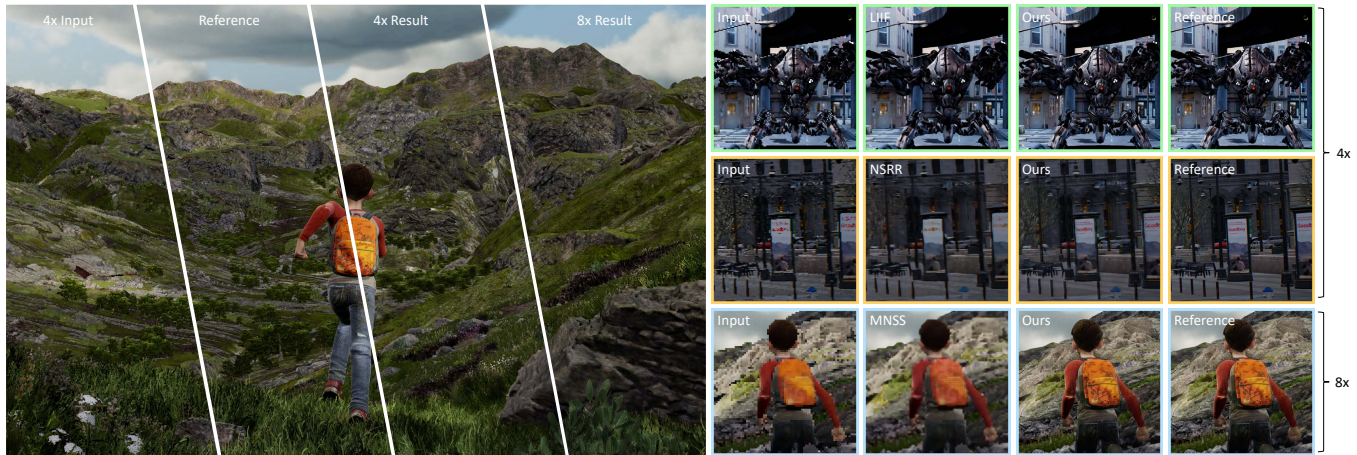State Key Lab of CAD&CG,
Zhejiang University
China

Figure 1: Our method achieves high-fidelity 4×4 **super-resolution images, significantly outperforming existing methods in performance and quality. Our method even succeeds in the extremely challenging** 8×8 **super-resolution task (bottom right), on which existing methods basically fail, thanks to our BRDF demodulation and multi-resolution fusion design to preserve high-frequency details. Zoom in for details.**

ABSTRACT

The workload of real-time rendering is steeply increasing as the demand for high resolution, high refresh rates, and high realism rises, overwhelming most graphics cards. To mitigate this problem, one of the most popular solutions is to render images at a low resolution to reduce rendering overhead, and then manage to accurately upsample the low-resolution rendered image to the target resolution, a.k.a. super-resolution techniques. Most existing methods focus on exploiting information from low-resolution inputs, such as historical frames. The absence of high frequency details in those LR inputs makes them hard to recover fine details in their high-resolution predictions. In this paper, we propose an efficient and effective super-resolution method that predicts high-quality upsampled reconstructions utilizing low-cost high-resolution auxiliary G-Buffers as additional input. With LR images and HR G-buffers as input, the network requires to align and fuse features at multi resolution levels. We introduce an efficient and effective H-Net architecture to solve this problem and significantly reduce rendering overhead without noticeable quality deterioration. Experiments show that our

*Equal contribution.
†Corresponding author.

method is able to produce temporally consistent reconstructions in 4×4 and even challenging 8×8 upsampling cases at 4K resolution with real-time performance, with substantially improved quality and significant performance boost compared to existing works.Project page: https://isaac-paradox.github.io/FuseSR/

CCS CONCEPTS

• **Computing methodologies → Rendering**.

KEYWORDS

super resolution, rendering, deep learning

ACM Reference Format:

1 INTRODUCTION

In the past few years, with the popularity of high-resolution and high-refresh-rate displays, as well as photographic realistic lighting and the advancement of real-time ray tracing techniques, the computational workload of real-time rendering has increased dramatically. The emergence of real-time raytracing has further increased the computational overhead of rendering for higher quality outputs. Even with the high-end consumer GPU, rendering high-quality images at 144 FPS and 4K resolution is still extremely challenging. As a result, users have to make trade-offs between rendering quality, resolution, and refresh rate.

A large number of techniques have been proposed to alleviate this problem. Real-time denoising techniques [Fan et al. 2021; Schied et al. 2017] render images at a low tracing budget and manage to reduce these images' noise levels to produce plausible results. Frame extrapolation methods [Guo et al. 2021; Zeng et al. 2021] focus on reconstructing accurate shading results from historical frames reprojected with motion vectors to accelerate rendering. Foveated rendering methods [Kaplanyan et al. 2019] propose to reduce the resolution at the periphery of users' vision without sacrificing perceived visual quality, thereby improving efficiency, but only for virtual reality headsets.

The most widely adopted and successful method is the super-resolution (SR) approaches, including DLSS [NVIDIA 2018], FSR [AMD 2021], XeSS [Intel 2022], etc. Users can reduce the resolution of rendered images to decrease rendering time and upsample the low-resolution (LR) rendered image to obtain the final high-resolution (HR) image. However, they mainly consider upsampling factors less than 2×2, which limits higher performance improvement. NSRR [Xiao et al. 2020] pursues a more promising task that produces high-quality 4×4-upsampled reconstruction in real-time by utilizing historical frames, yet it struggles with recovering accurate high-frequency texture details and cannot support real-time experience at resolutions higher than 1080p.

The results of NSRR demonstrate that high-resolution SR is a tough challenge. On the one hand, many high-fidelity details are lost even in historical frames. In theory, a 4×4 SR reconstruction requires

at least 16 historical frames to cover every pixel of the HR target fully, and such a long temporal window makes the history-reusing scheme basically infeasible in dynamic scenes. An intuitive solution is to utilize HR G-buffers that contain full-resolution information, of which the rendering cost is negligible and only sub-linearly increases. On the other hand, the network performance is also a critical concern for real-time SR and the neural network inference time increases rapidly w.r.t. the input resolution. Therefore, the need to increase feature resolution and reduce network bandwidth is a pair of contradictions that are difficult to resolve, which slows down the development of high-resolution SR.

In this paper, we present FuseSR, an efficient and effective real-time super-resolution technique that is able to offer high-fidelity 4×4 even 8×8 upsampled reconstruction with significantly improved quality and performance compared to existing works. Besides using historical information, we utilize HR G-buffer to provide per-pixel cues for the HR target. We further decompose the shading results into pre-integrated BRDF and demodulated irradiance components, and train a network to predict the HR irradiance, to strike a better balance between quality and efficiency. Most importantly, we propose *H-Net* architecture to resolve the contradictions between HR features and LR bandwidth. In H-Net, we incorporate pixel shuffling and unshuffling [Gharbi et al. 2016; Shi et al. 2016] to losslessly align HR features with LR inputs and fuse the features into the LR network backbone, while preserving high-fidelity HR details. Our contributions can be summarized as follows:

- Our method successfully utilizes high-resolution G-buffers to resolve the real-time super-resolution problem, which significantly outperforms existing methods in both time and quality. We are the first method to produce high-fidelity results in the challenging 8×8 super-resolution task.
- We propose H-Net, an efficient and effective network design to conduct lossless multi-resolution feature alignment and fusion with a low-resolution network backbone. We innovatively employ pixel shuffling and unshuffling pair into our network design to align and fuse multi-resolution features into the same screen space.
- We introduce pre-integrated BRDF demodulation to resolve the super-resolution problem, improving detail preservation and reducing the redundancy of G-buffers.

2 RELATED WORK

Real-time supersampling. In real-time rendering, each pixel of rendered images is point sampled. Therefore, the SR of rendered images can be conceived as a supersampling problem with upscaling. Supersampling-based antialiasing techniques [Akeley 1993; Young 2006] and temporal antialiasing methods [Karis 2014; Yang et al. 2020] manage to conduct supersampling in spatial and temporal domain. These aforementioned antialiasing techniques supersample without resolution changing. On the other hand, deep learning-based supersampling with upscaling has gained increasing attention recently. Deep learning super sampling (DLSS) [NVIDIA 2018] utilizes neural networks to upscale LR frames, significantly reducing the rendering cost of HR frames and enabling high-quality rendering at high resolution in real-time. It inspired a series of similar works, including FSR [AMD 2021], TAAU [Epic Games 2020a],

and XeSS [Intel 2022]. However, these methods focus on tasks with upsampling factors smaller than 2×2, limiting further performance improvement. NSRR [Xiao et al. 2020] is the closest to our method, which uses temporal dynamics and G-buffer to provide compelling results in the challenging 4×4 upsampling case, but it cannot accurately recover HR details and is unable to support real-time rendering at high resolutions such as 2K and 4K. MNSS [Yang et al. 2023] also leverages historical frames, and achieves competitive runtime performance due to its lightweight network design.

Pixel Shuffling. ESPCN [Shi et al. 2016] firstly designs pixel shuffling as an efficient upscaling operation in their super-resolution network, which keeps most convolutional layers in low resolution to reduce network computational overhead. Gharbi et al. [2016] further design a pixel unshuffling-shuffling pair in their denoising network architecture, with the purpose of converting pixel-wise noise patterns into channel-wise for better denoising processing. Inspired by these methods, our approach adopt pixel shuffling for high speed and pixel unshuffling for the alignment and fusion of multi-resolution input features.

BRDF demodulation. Materials with fine details can increase rendering realism but also make reconstruction tasks (e.g., denoising and supersampling) more challenging. Demodulating BRDF is a common practice for preserving details in reconstruction tasks. Bako et al. [2017] and SVGF [Schied et al. 2017] demodulate the diffuse albedo from the noisy image and then modulate it with the denoised result to alleviate the blurring problem. Guo et al. [2021] found that such demodulation was also beneficial for extrapolated rendering. Pre-integrated BRDF demodulation [Zhuang et al. 2021] is also proven effective for real-time denoising. Inspired by these methods, our approach introduces demodulation similar to [Zhuang et al. 2021] to decompose the color frames SR into the SR tasks of corresponding pre-integrated BRDF maps and demodulated irradiance maps, wherein the demodulated irradiance map tends to be smoother than the original color, thus reducing the SR difficulty.

3 METHOD

The goal of our work is to reconstruct upsampled HR frames $\hat{I}^{HR}$ from the corresponding LR frames I^{LR} in real-time rendering. Unfortunately, the SR problem that relied entirely on LR color frames is ill-posed because of the lack of HR details. Inspired by previous works [Guo et al. 2021], we take HR G-buffers as SR cues to make the problem more tractable. G-buffer is a commonly used rendering byproduct containing rich scene information (e.g., depths, normals, and texture details), and its acquisition is significantly cheaper (several milliseconds for each 1080p frame) than heavy shading and potential post-processing tasks.

To utilize material information from G-Buffer, we employ pre-integrated BRDF demodulation (Section 3.1) to explicitly filter out HR details, turning the color frame SR to an easier demodulated irradiance SR problem. We further design our *H-Net* architecture employing pixel shuffling operations (Section 3.2) to effectively and efficiently align and fuse HR and LR information. Our design demonstrates significantly improved quality and performance compared with other advanced works.

To be precise, we describe our task as follows:

$$\hat{I}^{HR} = \textbf{SuperResolution}(I^{LR}, G^{LR}, G^{HR}), \qquad (1)$$

where G^{LR} and G^{HR} denote LR and HR G-buffers respectively, which are taken as auxiliary input features to enrich the input information for better predictions.

3.1 BRDF Demodulation for Superresolution

Today's production-ready 3D scenes are becoming more and more exquisite, making the superresolution task, especially those with high-frequency features, more challenging. Inspired by Zhuang et al. [2021], we perform BRDF demodulation to filter out high-frequency material details for better overall quality and detail preservation. Specifically, we reformulate the rendering equation [Kajiya 1986] into the multiplication of the pre-integrated BRDF term $F_\beta(\omega_o)$ and the demodulated irradiance term $L_D(\omega_o)$:

$$L_o(\omega_o) = \int_\Omega f_r(\omega_i, \omega_o) L_i(\omega_i) \cos \theta_i \mathrm{d}\omega_i \qquad (2)$$

$$F_\beta(\omega_o) = \int_\Omega f_r(\omega_i, \omega_o) \cos \theta_i \mathrm{d}\omega_i, \ L_D(\omega_o) = \frac{L_o(\omega_o)}{F_\beta(\omega_o)} \qquad (3)$$

where ω_i, ω_o denotes the incoming and outgoing directions, respectively, $f_r(\omega_i, \omega_o)$ represents the bidirectional reflectance distribution function (BRDF) at the shading point, the lighting function $L_i(\omega_i)$ describes incident radiance at the shading point, $\cos \theta_i$ is the cosine term, and $L_o(\omega_o)$ is the outgoing radiance. This demodulation decomposes the radiance of a pixel into two terms: $F_\beta(\omega_o)$ and $L_D(\omega_o)$. Hence the superresolution task turns into estimating the corresponding HR F_β and HR L_D maps.

We adopt the precomputation approach proposed by Karis et al. [2013] (known as *split-sum approximation*) to acquire F_β maps at a negligibly low cost. In the precomputation stage, the BRDF integrals to each normal and light direction combination on varying roughness values are computed and stored in a 2D lookup texture (LUT). After that, we can easily obtain F_β maps with arbitrary resolutions by querying the LUT according to each pixel's roughness and view direction that are provided in the G-buffers. We refer readers to the original paper [Karis 2013] for more details.

Then, we leverage a neural network Φ to predict the HR demodulated irradiance map $\hat{L}_D^{HR}$ and multiply it with the HR pre-integrated BRDF map F_β^{HR} pixel-by-pixel to obtain the SR outcome. Thus Eq. (1) can be rewritten as:

$$\hat{L}_D^{HR} = \Phi(L_D^{LR}, G^{LR}, G^{HR}), \ \hat{I}^{HR} = F_\beta^{HR} \odot \hat{L}_D^{HR}, \qquad (4)$$

where $\odot$ denotes pixel-wise multiplication. The LR demodulated irradiance map L_D^{LR} can be easily computed by dividing the LR color map I^{LR} by the LR pre-integrated BRDF map F_β^{LR} pixel-by-pixel, while F_β^{HR} can be easily pre-computed from HR G-buffers G^{HR}. Note that we omit the emitted radiance term in the rendering equation because its HR version is available in the G-buffers.

Please refer to our supplementary for the visualization of F_β map with high-frequency details and L_D map smoother than the original pixel color. We believe that estimating the smoother L_D map instead of the original color frame is conducive to improving the quality and generalizability. Our experiments confirmed this choice (see Section 5.4.1).
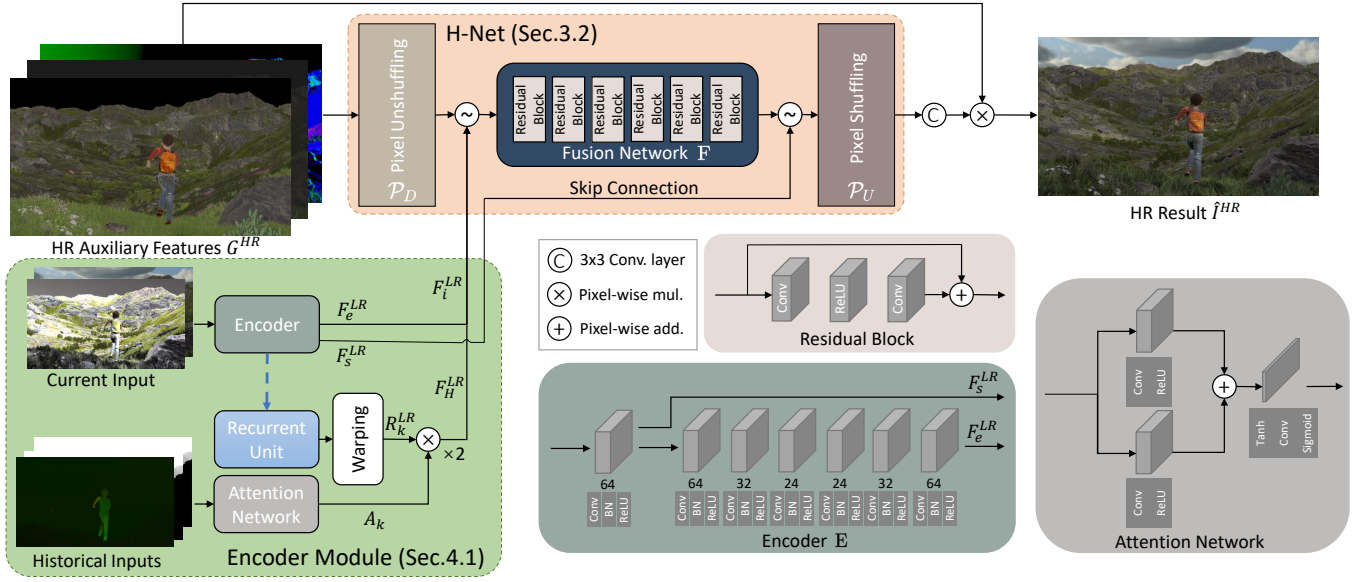
Figure 2: The pipeline of our method. We perform BRDF demodulation to turn the SR of shading images into the prediction of the HR demodulated irradiance map and acquisition of the HR pre-integrated BRDF map. An effective and efficient *H-net* is introduced to fuse LR features with HR G-buffers to reconstruct the HR demodulated irradiance map and remodulate it with the HR pre-integrated BRDF map that can be acquired efficiently to obtain the final SR outcome.

3.2 H-Net: An Effective and Efficient Network for Multi-Resolution Alignment and Fusion

Given that our network takes multi-resolution features (LR image and HR G-buffers) as input, to make full use of the HR auxiliary inputs, an efficient network is required to organize the features at different resolution levels. Aligning pixels that share the same screen space position can preserve correct spatial correlation between multi-resolution input features. After that, our network fuses the aligned multi-resolution features to finish the SR task.
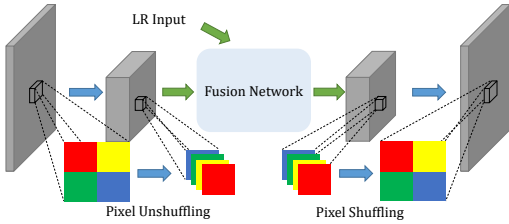

Figure 3: Architecture of H-Net.

Multi-resolution feature alignment. To align pixels sharing the same screen space position, *upsampling* and *pooling* are two common strategies, where the former aligns at HR level and the latter aligns at LR level. Considering that the performance of convolutional networks degrades sharply as the input resolution increases, the upsampling alignment contradicts with the need of real-time performance, while pooling is a more feasible choice.

Pooling operations are commonly used in neural networks, including maximum pooling and average pooling. However, these pooling operations inevitably damage the spatial details such as HR edges and textures, which are key information for SR quality improvements. Therefore, instead of lossy pooling operations, we adopt pixel unshuffling operation [Gharbi et al. 2016; Shi et al. 2016] to align an HR feature to LR without information loss. We find that pixel unshuffling can losslessly shrink an HR feature map into LR space, converting pixel-wise spatial information into channel-wise deep information. Specifically, this operation divides the HR map into blocks of size $r \times r$ (r is the downscaling factor) and concatenates the features of all pixels within each block to form pixels of the LR version, *i.e.* transforming a map of shape $[C, H * r, W * r]$ into an LR map of shape $[C * r * r, H, W]$ without information loss.

H-Net. We propose an *H-Net* architecture with a pixel unshuffling-shuffling pair, to efficiently align and fuse LR and HR information to faithfully preserve HR details during the alignment and fusion. The architecture of H-Net is shown in Fig. 3:

(1) We use pixel unshuffling $\mathcal{P}_D$ to downscale G^{HR} and concatenate it with other LR inputs.

(2) The concatenated feature is fed into a fusion network backbone $\mathbf{F}$. Note that $\mathbf{F}$ runs at LR level, which prevents significant HR computational overhead.

(3) The output of $\mathbf{F}$ is transformed to HR space using pixel shuffling $\mathcal{P}_U$ to obtain the HR output $\hat{L}_D^{HR}$.

Formally, the process can be expressed as follows:

$$\hat{L}_D^{HR} = \mathcal{P}_U\left(\mathbf{F}\left(\left[\mathbf{E}\left(\left[L_D^{LR}, G^{LR}\right]\right), \mathcal{P}_D\left(G^{HR}\right)\right]\right)\right), \quad (5)$$

where $[\cdot, \cdot]$ represents concatenation, and $\mathbf{E}$ is the encoder used to obtain the LR feature map (Section 4). The name "H-Net" is

motivated by the shape of the network with two HR ends and an LR bottleneck, resembling an "H".

With the use of pixel unshuffling, our method can faithfully preserve the HR details, thus facilitating high-quality SR outcomes. Moreover, since neighboring pixels are usually highly correlated, aggregating neighboring pixels of the HR map together via $\mathcal{P}_D$ allows obtaining more compact implicit representations in the following fusion network, which is beneficial for reducing data redundancy and enhancing efficiency. Our experiments show that our alignment strategy even achieves better quality than the naïve HR upsampling alignment strategy (see Section 5.4.2).

4 NETWORK AND TRAINING

In this section, we first provide the specific architecture of our network in Section 4.1, and then describe details of the implementation and training in Section 4.2.

4.1 Network Architecture

Here we explain the architectural details of each component involved in Eq. (5), including the encoder $\mathbf{E}$, fusion network $\mathbf{F}$, and a pixel unshuffling-shuffling pair $\mathcal{P}_D$ and $\mathcal{P}_U$. Unless otherwise stated, all convolutional layers are set by default to a convolution with a 3×3 kernel size, a stride of 1, zero padding, and a subsequent ReLU activation. Please refer to our supplementary material for detailed network configurations.

Encoder. The encoder module takes LR irradiance and G-buffers as input and outputs an LR feature map as part of the input of our H-Net (Eq. (5)). Following existing works , we also utilize LR historical frames to encourage temporal consistency. The architecture of the encoder is shown in the bottom left corner of Fig. 2, and please refer to our supplementary material for details on how we encode LR current frame and historical frames.

Formally, the encoder takes the LR irradiance along with G-buffers of current frame and 2 previous frames as input, and output 2 LR feature maps F_s^{LR} and F_i^{LR}:

$$F_s^{LR}, F_i^{LR} = \mathbf{E}\left(\left[L_{D_i}^{LR}, G_i^{LR}, \left\{L_{D_k}^{LR}, G_k^{LR}\right\}_{k \in \{i-1, i-2\}}\right]\right) \quad (6)$$

where i is the current frame index, F_s^{LR} is the output of the first layer of $\mathbf{E}$ used for skip connection later, and F_i^{LR} is the final output as an input of the fusion network.

Fusion network. In our fusion network $\mathbf{F}$, the LR feature from encoder F_i^{LR}, and the unshuffled HR auxiliary features G^{HR} are concatenated and fed into a subsequent network $\mathbf{F}$ to obtain an LR fused feature map F_f^{LR}:

$$F_f^{LR} = \mathbf{F}\left(\left[F_i^{LR}, \mathcal{P}_D\left(G^{HR}\right)\right]\right). \quad (7)$$

Final upscaling module. In this module, we skip-connect the first layer output F_s^{LR} of the encoder $\mathbf{E}$ with the fused feature map F_f^{LR} and then upscale this concatenated feature map via the pixel shuffling operation $\mathcal{P}_U$. Finally, the upscaled feature map is processed by a single-layer convolutional network to obtain the RGB prediction

of demodulated irradiance $\hat{L}_D^{HR}$ (Section 3.1):

$$\hat{L}_D^{HR} = \mathbf{Conv}\left(\mathcal{P}_U\left(\left[F_s^{LR}, F_f^{LR}\right]\right)\right), \quad (8)$$

After obtaining $\hat{L}_D^{HR}$, we can compute the final color prediction $\hat{I}^{HR}$ by remodulating with F_β^{HR} as described in Eq. (4).

4.2 Training

We train our network with the supervision of ground truth high-resolution images, and the training process is end-to-end.

L_1 *loss.* We directly apply L_1 loss between HR ground truth I^{HR} and the predicted HR image $\hat{I}^{HR}$ to supervise the training:

$$\mathcal{L}_{\text{color}} = \|\hat{I}^{HR} - I^{HR}\|_1. \quad (9)$$

Perceptual loss. Introduced by Johnson et al. [2016], we use a pretrained VGG-16 network to compute perceptual loss to enhance semantic consistency:

$$\mathcal{L}_{\text{perceptual}} = \sum_{i \in V} \|\text{VGG}_i(\hat{I}^{HR}) - \text{VGG}_i(I^{HR})\|_2, \quad (10)$$

where VGG_i represents the i-th layer of pre-trained VGG network, and V denotes the set of selected layers.

SSIM loss. Following NSRR [Xiao et al. 2020], we also incorporate structural similarity index (SSIM) [Wang et al. 2004] as an additional loss function:

$$\mathcal{L}_{\text{strutural}} = 1 - \text{SSIM}(\hat{I}^{HR}, I^{HR}), \quad (11)$$

Total loss. To summarize, the total loss is the weighted combination of all losses mentioned above:

$$\mathcal{L} = \mathcal{L}_{\text{color}} + \lambda_p \mathcal{L}_{\text{perceptual}} + \lambda_s \mathcal{L}_{\text{strutural}}. \quad (12)$$

We empirically set $\lambda_p = 0.5$ and $\lambda_s = 0.05$ in our experiments.

5 EXPERIMENT

In this section, we will demonstrate the comprehensive experimental results of our method. We first introduce implementation details of our network and datasets used in training and testing (Section 5.1). Then, we compare our method with state-of-the-art methods in quality and performance (Section 5.2). We further make a discussion on the performance and quality of integrating our method into rendering pipelines compared to native HR rendering in Section 5.3. At last, experiments are conducted to validate the effectiveness of each design (Section 5.4).

5.1 Implementation Details and Datasets

Implementation details. Our model is implemented and trained using PyTorch [Paszke et al. 2019]. All training and testing are performed on a single NVIDIA RTX 3090 GPU. For the best trade-off between performance and quality, we evaluate two implementations of our FuseSR model, namely *Ours* and *Ours ʄ*. "Ours" version provides full network implementation with optimal quality. "Our ʄ" version is more performance-oriented. It cuts off the history reusing module in the encoder (Section 4.1), reduces the number of hidden channels of all layers in fusion network $\mathbf{F}$ by half, and replaces all convolutional layers in $\mathbf{F}$ with faster DWS layers [Sandler et al. 2018] to improve the performance at a slight sacrifice of quality.

Table 1: Left: Quality comparisons with baselines in 4×4 upsampling. The top 3 best results are highlighted with gold, silver, and bronze. Right: Quality comparisons in the challenging 8×8 upsampling.

		Ours	Ours ⚡	NSRR	MNSS	LIIF	FSR	XeSS	Ours-8x	NSRR-8x	MNSS-8x
PSNR (dB)	Kite	32.33	31.22	27.74	28.00	26.47	29.12	28.30	30.21	25.00	25.72
	Showdown	36.32	31.42	30.27	29.17	30.33	26.29	29.31	33.61	29.17	25.62
	Slay	37.02	34.41	35.42	35.39	31.12	32.39	34.94	34.26	32.12	33.47
	City	28.94	28.66	27.65	28.23	26.56	26.63	27.15	27.20	25.95	26.46
SSIM	Kite	0.933	0.900	0.832	0.829	0.817	0.887	0.893	0.899	0.765	0.770
	Showdown	0.976	0.949	0.945	0.914	0.942	0.866	0.917	0.955	0.914	0.813
	Slay	0.972	0.958	0.962	0.963	0.962	0.928	0.944	0.957	0.939	0.943
	City	0.921	0.901	0.899	0.896	0.874	0.836	0.888	0.916	0.873	0.873

Datasets. We have constructed a large-scale dataset using four virtual scenes selected from Unreal Engine marketplace[1] We select 2 scenes from Unreal Engine 4 (Kite and Showdown), and 2 scenes from Unreal Engine 5 (Slay and City). These scenes contain extensively complex geometry and lighting conditions with dynamic objects. Each scene contains 1080 continuous frames, of which 960 frames are used for training and 120 are used for testing. To show our method's ability for high-quality rendering, the 2 scenes from UE 5 are rendered by real-time raytracing to achieve photorealistic appearances. We choose 4K (3840×2160) as the resolution of the target HR frame and the LR frames are downscaled according to scale factor. All frames are generated using UE 4 [2020b] and 5 [2021] with customized shaders to compute the required G-buffers, pre-integrated BRDF, and motion vectors.

Metrics. Our evaluation comprises two aspects: performance and quality. We report the runtime of networks in milliseconds (ms) as a straightforward metric in performance. In terms of quality, we report two widely-used image metrics: peak signal-to-noise ratio (PSNR) and structural similarity index (SSIM) [Wang et al. 2004]. For both PSNR and SSIM, higher is better.

5.2 Results and Comparisons

5.2.1 Quality evaluation. We compare our method with several state-of-the-art super-resolution methods in both academia and industry, including SOTA single image super-resolution method LIIF [Chen et al. 2021], real-time rendering super-resolution methods NSRR [Xiao et al. 2020] and MNSS [Yang et al. 2023], and methods widely used in the gaming industry including AMD's FidelityFX™ Super Resolution (FSR) [AMD 2021] and Intel Xe Super Sampling (XeSS) [Intel 2022].

In Table 1, we compare PSNR and SSIM metrics averaged over all frames from 4 scenes of our dataset . Our method significantly outperforms other baselines in all scenes quantitatively. We also provide qualitative comparisons in Fig. 7. Our method faithfully produces HR details such as sharp edges and complex textures, owing to our exploitation of BRDF demodulation and effective H-Net design.

5.2.2 Runtime performance. The performance of a super-resolution method is crucial for its application to real-time high-resolution rendering. After training, the optimized models are accelerated

[1]https://unrealengine.com/marketplace

by NVIDIA TensorRT [2018] with 16-bit mixed precision for optimal inference speed. In Table 2, we report the total runtime of our method and baselines at different resolutions. Benefiting from our carefully designed H-Net architecture, both of our two versions achieve superior performance to NSRR at all configurations.

MNSS achieves competitive runtime performance due to its lightweight network design, especially at low resolutions. However, it requires network computations at HR level, leading to a more steep increase in running time compared to ours. With G-buffer generation time included, Ours ⚡surpasses MNSS above 2K resolution.

The performance of our method is highly dependent on the upscaling factor, because our fusion network runs at LR level thanks to our pixel unshuffling alignment strategy. "Ours-8x" achieves superior performance to "Ours", especially for high resolutions.

"Ours ⚡" version indeed leads to a slight decrease in quality, which is reasonable due to the reduced network capacity. Nevertheless, it still performs on par with or better than other baselines. Fig. 4 displays the trade-off between performance and quality.

Table 2: Comparison of total runtime and HR G-buffer generation time (in milliseconds) for SR tasks (8×8 for "Ours-8x" and 4×4 for others) with different target resolutions. Results are tested on an NVIDIA RTX 3090 GPU.

	720p	1080p	2K	4K
HR G-buffer	0.83	0.93	1.97	2.35
Ours	6.21	8.44	15.09	33.93
Ours-8x	6.20	7.57	8.79	16.20
Ours ⚡	2.66	2.88	3.96	7.82
NSRR	13.53	26.29	64.02	149.20
MNSS	2.26	3.57	5.52	11.29

5.2.3 Upsampling Factor. Besides 4×4 super-resolution, we also evaluate our method on a more challenging 8×8 task, which requires the network to predict 64 HR sub-pixel colors from a single LR pixel. Such a high upsampling rate makes it nearly impossible for previous methods with the absence of HR cues to recover any details, while our method still predicts high-fidelity results thanks to the demodulation and multi-resolution fusion. Table 1 (Right) and Fig. 8 demonstrates quantitative and qualitative results of our method and SOTA baselines.
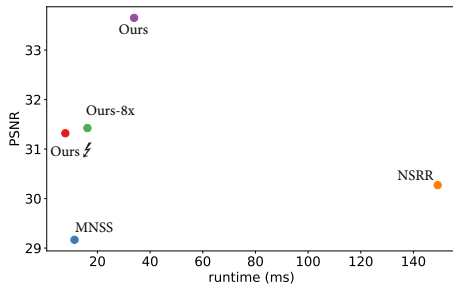
Figure 4: Comparisons on the trade-off between performance and quality.

5.3   Discussion on Real-time Rendering

G-buffer generation. We test G-buffer generation time by recording the rendering state via the UE built-in profiling tool. For each scene, we measure the average G-buffer time on a sequence of dynamic frames and take 10 samples to cover as many scenarios as possible. Notably, G-buffer generation time is affected by various factors and there is a variance between certain frames within four orders of magnitude ranging from 0.01 ms to less than 10 ms. In general, the average G-buffer time is significantly lower than network time (as reported in the first row of Table 2). In modern game engines, simplification techniques, such as LOD or new techniques like Nanite in UE5, can further reduce the overhead of G-Buffer generation to a stably low cost.
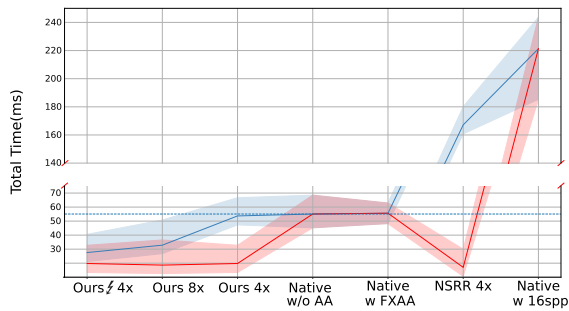

Figure 5: Comparison of runtime between our method and native rendering of HR image at 4K resolution. Blue lines denote the total runtime (LR rendering + G-buffer generation + network inference), while red lines denote the overhead within the rendering pipeline (LR rendering + G-buffer). Results are taken from Slay scene in UE5.

Comparisons to HR native rendering. The ultimate goal of SR for real-time rendering is to reduce computational overhead by avoiding native rendering of HR images by the rendering engine. The performance of native rendering is affected by multiple factors including resolution and anti-aliasing options. In Fig. 5, we compare the runtime of HR native rendering with the total runtime of rendering an LR image and then super-resolving it into HR by our method. We report native rendering runtimes with different anti-aliasing levels (w/o AA, FXAA, and SSAA), and our results with

different network configurations (Ours and Ours ⚡) and different SR upscaling factors (4x and 8x). Results show that integrating our method into the rendering pipeline indeed reduces computational overhead compared to native rendering.

Scene complexity. The native rendering overhead typically depends on the complexity of scenes and lighting conditions, while the inference time of SR network basically remains constant among varying scenes. Integrating SR into rendering pipelines can increase the potential of designing more complex scenes for modern games without noticeable degradation of rendering performance.

5.4   Ablation Studies

5.4.1   Network modules. In Table 3, we report ablation experiments on our BRDF demodulation (Section 3.1) and HR G-buffer fusion (Section 3.2). The results confirm the effectiveness of our design.

Table 3: Ablation studies for HR G-buffer fusion and BRDF demodulation. Results in the table are averaged from experiments on Kite and Slay scenes.

HR G-Buffer	Demodulation	PSNR(dB)	SSIM
✗	✗	31.88	0.891
✓	✗	33.74	0.941
✗	✓	33.05	0.926
✓	✓	34.67	0.952

5.4.2   Alignment strategy. Table 4 and Fig. 6 shows the comparisons between different alignment strategies used before the fusion network. Our strategy significantly outperforms maximum pooling and average pooling due to the preservation of HR details. Our strategy even outperforms the upsampling alignment strategy (where the fusion network runs much slower at HR level), showing the effectiveness of compact LR implicit representations.

Table 4: Ablation studies for different alignment strategies on 2 scenes.

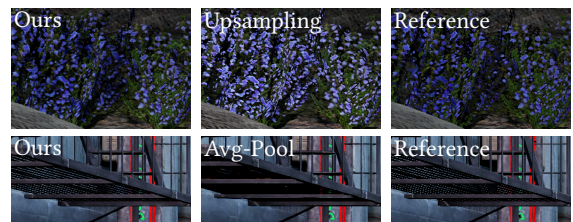|	Ours	Avg-Pool	Max-Pool	Upsampling
Kite	32.33	32.14	31.87	32.09
Slay	37.02	36.32	36.11	36.69

Figure 6: Ablation studies for alignment strategies. Upsampling leads to color bias, while spatial pooling leads to the loss of thin structures.

6 DISCUSSION AND CONCLUSION

Integration cost. While HR G-buffers provide a good guidance for upscaling and the demodulation further helps with the quality, these additional inputs require major modifications to modern game engines to integrate FuseSR. For example, to provide pre-integrated BRDF term $F_\beta(\omega_o)$, the engine should generate pre-integrated BRDF LUT for each material asset. To reduce integration costs, some rational trade-offs may be considered such as using FuseSR without demodulation or replacing $F_\beta(\omega_o)$ with albedo.

Material Generalization. Split-sum approximation offers an efficient means for BRDF demodulation, but it also limits the material types we can support. Materials that violate the assumptions of split-sum approximation, such as translucent and anisotropic materials, are not available in our method. Therefore, finding a more general BRDF demodulation method is an important direction for our future research.

Potential of H-Net. We believe that our H-Net design are flexible and scalable, with the potential to be extended to more resolution levels and more multi-resolution tasks such as multi-scale object detection. We leave it as an interesting future work.

Conclusion. We present FuseSR, an efficient and effective super-resolution network that predicts high-quality 4×4 (even 8×8) upsampled reconstructions according to the corresponding low-resolution frames. With introducing pre-integrated BRDF demodulation and H-Net design, our method achieves a new SOTA for real-time superresolution. The experiments show that our method not only strikes an outstanding balance strikes an excellent balance between quality and performance, but also exhibits excellent generalizability and temporal stability. We hope our work will stimulate further developments of neural superresolution.

ACKNOWLEDGMENTS

REFERENCES

Kurt Akeley. 1993. Reality engine graphics. In *Proceedings of the 20th annual conference on Computer graphics and interactive techniques.* 109–116.

AMD. 2021. *AMD FidelityFX™ Super Resolution.* https://www.amd.com/en/technologies/fidelityfx-super-resolution/

Steve Bako, Thijs Vogels, Brian McWilliams, Mark Meyer, Jan Novák, Alex Harvill, Pradeep Sen, Tony Derose, and Fabrice Rousselle. 2017. Kernel-predicting convolutional networks for denoising Monte Carlo renderings. *ACM Trans. Graph.* 36, 4 (2017), 97–1.

Yinbo Chen, Sifei Liu, and Xiaolong Wang. 2021. Learning continuous image representation with local implicit image function. In *Proceedings of the IEEE/CVF conference on computer vision and pattern recognition.* 8628–8638.

Epic Games. 2020a. *Screen Percentage with Temporal Upscale in Unreal Engine.* https://docs.unrealengine.com/en-US/screen-percentage-with-temporal-upscale-in-unreal-engine/

Epic Games. 2020b. *Unreal Engine.* https://www.unrealengine.com/

Epic Games. 2021. Unreal Engine. https://www.unrealengine.com/en-US/unreal-engine-5.

Hangming Fan, Rui Wang, Yuchi Huo, and Hujun Bao. 2021. Real-time Monte Carlo Denoising with Weight Sharing Kernel Prediction Network. In *Computer Graphics Forum,* Vol. 40. Wiley Online Library, 15–27.

Michaël Gharbi, Gaurav Chaurasia, Sylvain Paris, and Frédo Durand. 2016. Deep joint demosaicking and denoising. *ACM Transactions on Graphics (ToG)* 35, 6 (2016), 1–12.

Jie Guo, Xihao Fu, Liqiang Lin, Hengjun Ma, Yanwen Guo, Shiqiu Liu, and Ling-Qi Yan. 2021. ExtraNet: real-time extrapolated rendering for low-latency temporal supersampling. *ACM Transactions on Graphics (TOG)* 40, 6 (2021), 1–16.

Intel. 2022. *Intel Xe Super Sampling.* https://www.intel.com/content/www/us/en/products/docs/arc-discrete-graphics/xess.html/

Justin Johnson, Alexandre Alahi, and Li Fei-Fei. 2016. Perceptual losses for real-time style transfer and super-resolution. In *European conference on computer vision.* Springer, 694–711.

James T Kajiya. 1986. The rendering equation. In *Proceedings of the 13th annual conference on Computer graphics and interactive techniques.* 143–150.

Anton S Kaplanyan, Anton Sochenov, Thomas Leimkühler, Mikhail Okunev, Todd Goodall, and Gizem Rufo. 2019. DeepFovea: Neural reconstruction for foveated rendering and video compression using learned statistics of natural videos. *ACM Transactions on Graphics (TOG)* 38, 6 (2019), 1–13.

Brian Karis. 2013. Real shading in unreal engine 4. In *SIGGRAPH Courses: Physically Based Shading in Theory and Practice.*

Brian Karis. 2014. High Quality Temporal Anti-Aliasing. In *SIGGRAPH Courses: Advances in Real-Time Rendering.*

NVIDIA 2018. *Deep Learning Super Sampling (DLSS) Technology | NVIDIA.* NVIDIA. https://www.nvidia.com/en-us/geforce/technologies/dlss/

NVIDIA. 2018. *TensorRT.* https://developer.nvidia.com/tensorrt/

Adam Paszke, Sam Gross, Francisco Massa, Adam Lerer, James Bradbury, Gregory Chanan, Trevor Killeen, Zeming Lin, Natalia Gimelshein, Luca Antiga, et al. 2019. Pytorch: An imperative style, high-performance deep learning library. *Advances in neural information processing systems* 32 (2019).

Mark Sandler, Andrew Howard, Menglong Zhu, Andrey Zhmoginov, and Liang-Chieh Chen. 2018. Mobilenetv2: Inverted residuals and linear bottlenecks. In *Proceedings of the IEEE conference on computer vision and pattern recognition.* 4510–4520.

Christoph Schied, Anton Kaplanyan, Chris Wyman, Anjul Patney, Chakravarty R Alla Chaitanya, John Burgess, Shiqiu Liu, Carsten Dachsbacher, Aaron Lefohn, and Marco Salvi. 2017. Spatiotemporal variance-guided filtering: real-time reconstruction for path-traced global illumination. In *Proceedings of High Performance Graphics.* 1–12.

Wenzhe Shi, Jose Caballero, Ferenc Huszár, Johannes Totz, Andrew P Aitken, Rob Bishop, Daniel Rueckert, and Zehan Wang. 2016. Real-time single image and video super-resolution using an efficient sub-pixel convolutional neural network. In *Proceedings of the IEEE conference on computer vision and pattern recognition.* 1874–1883.

Zhou Wang, Alan C Bovik, Hamid R Sheikh, and Eero P Simoncelli. 2004. Image quality assessment: from error visibility to structural similarity. *IEEE transactions on image processing* 13, 4 (2004), 600–612.

Lei Xiao, Salah Nouri, Matt Chapman, Alexander Fix, Douglas Lanman, and Anton Kaplanyan. 2020. Neural supersampling for real-time rendering. *ACM Transactions on Graphics (TOG)* 39, 4 (2020), 142–1.

Lei Yang, Shiqiu Liu, and Marco Salvi. 2020. A survey of temporal antialiasing techniques. In *Computer graphics forum,* Vol. 39. Wiley Online Library, 607–621.

Sipeng Yang, Yunlu Zhao, Yuzhe Luo, He Wang, Hongyu Sun, Chen Li, Binghuang Cai, and Xiaogang Jin. 2023. MNSS: Neural Supersampling Framework for Real-Time Rendering on Mobile Devices. *IEEE Transactions on Visualization and Computer Graphics* (2023), 1–14. https://doi.org/10.1109/TVCG.2023.3259141

Peter Young. 2006. *Coverage sampled anti-aliasing.* Technical Report. NVIDIA Corporation.

Zheng Zeng, Shiqiu Liu, Jinglei Yang, Lu Wang, and Ling-Qi Yan. 2021. Temporally Reliable Motion Vectors for Real-time Ray Tracing. In *Computer Graphics Forum*, Vol. 40. Wiley Online Library, 79–90.

Tao Zhuang, Pengfei Shen, Beibei Wang, and Ligang Liu. 2021. Real-time Denoising Using BRDF Pre-integration Factorization. In *Computer Graphics Forum*, Vol. 40. Wiley Online Library, 173–180.
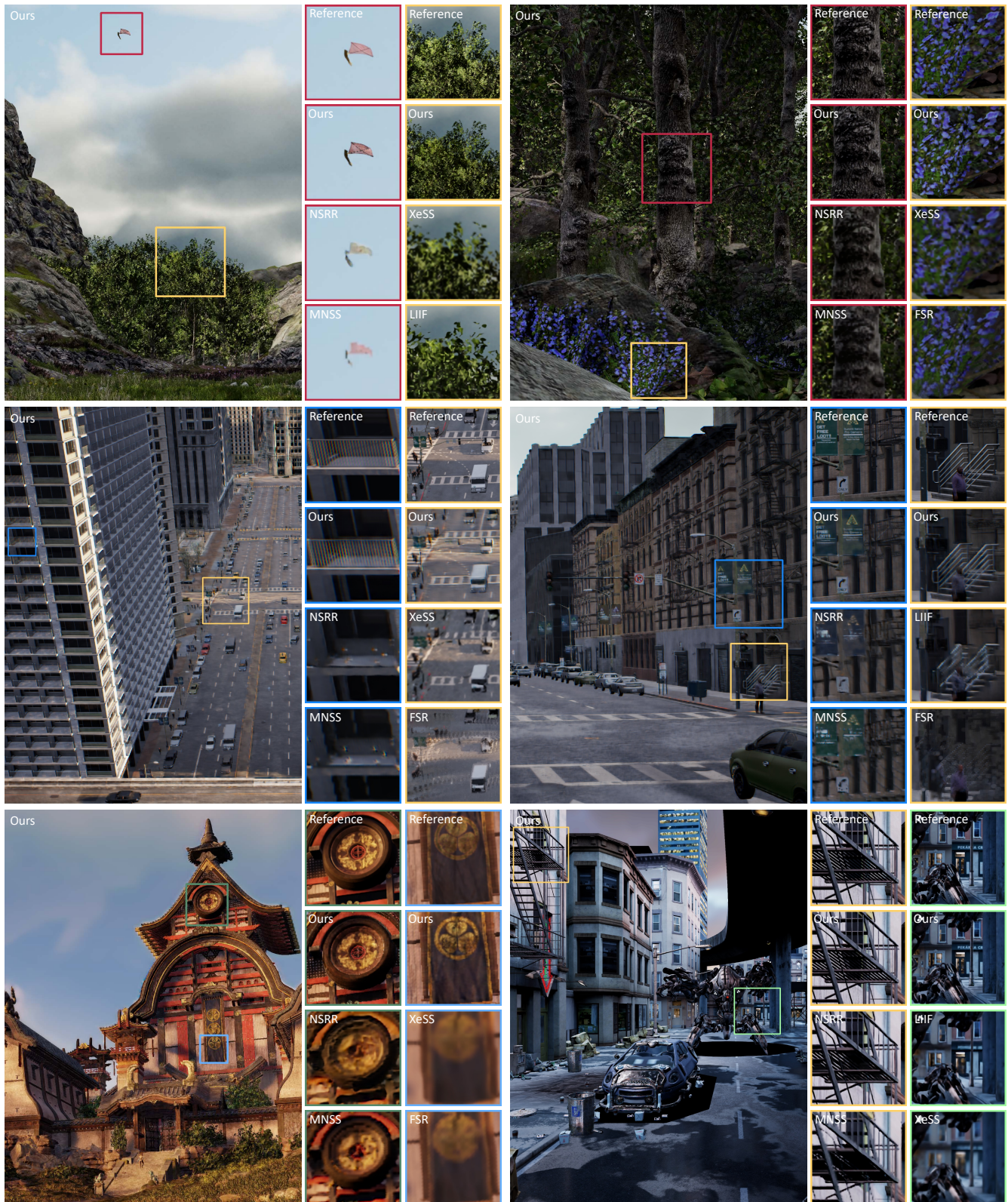
Figure 7: Comparisons of 4×4 **super-resolution between our method and baseline methods in** Kite, City, Slay **and** Showdown **scenes. Full images of reference and baselines are presented in the supplementary material.**
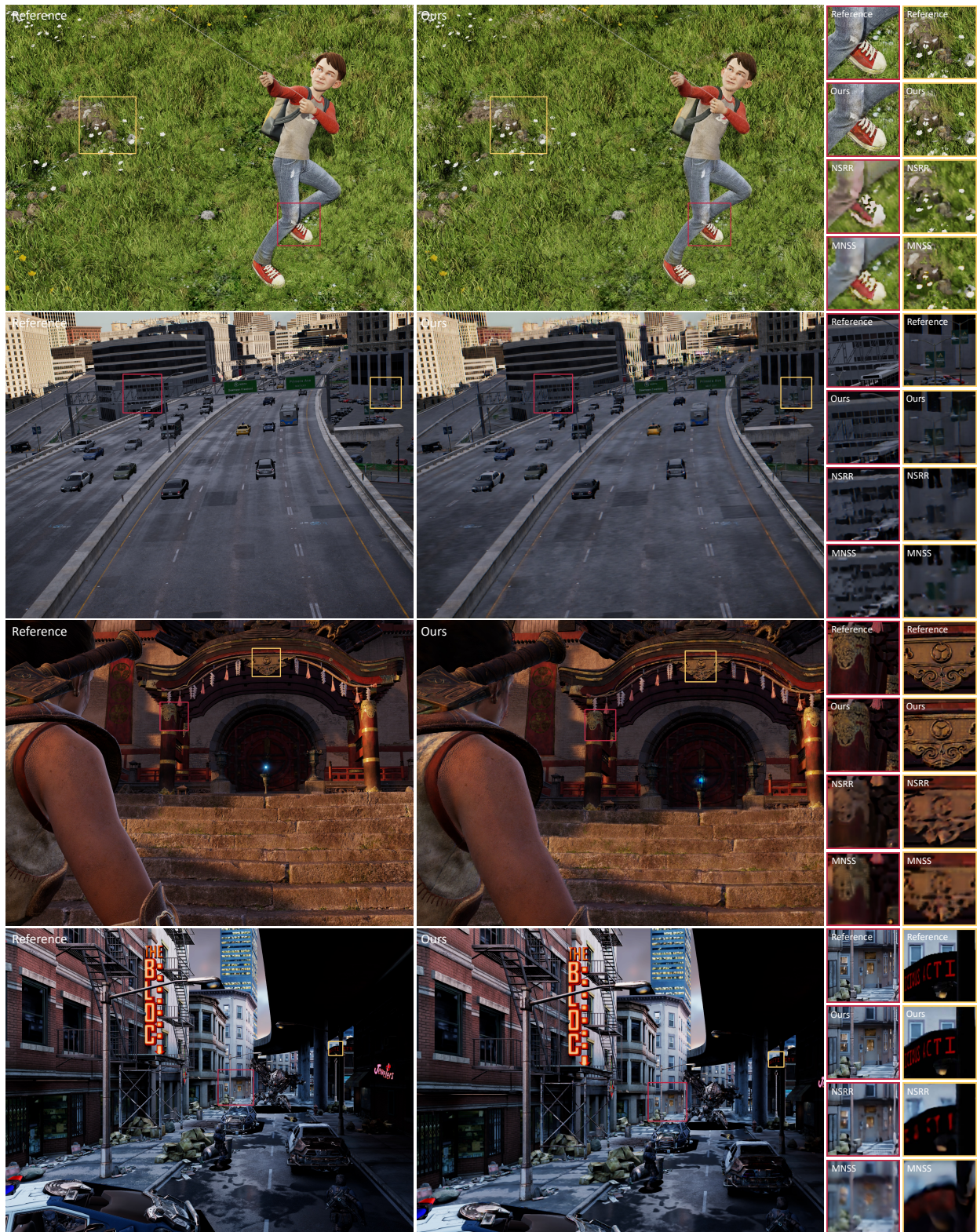
Figure 8: Comparisons of 8×8 **super-resolution between our method and baseline methods in** Kite, City, Slay **and** Showdown **scenes.**